ARL-TR-9540 ● SEP 2022

DEVCOM ARMY RESEARCH LABORATORY

Modeling the Rebound of Ballistic Roma Plastilina No. 1 Clay

by Timothy G Zhang, Mary J Graham, and Sikhanda S Satapathy

NOTICES

Disclaimers

The findings in this report are not to be construed as an official Department of the Army position unless so designated by other authorized documents.

Citation of manufacturer's or trade names does not constitute an official endorsement or approval of the use thereof.

Destroy this report when it is no longer needed. Do not return it to the originator.

ARL-TR-9540 ● SEP 2022

Modeling the Rebound of Ballistic Roma Plastilina No. 1 Clay

Timothy G Zhang and Sikhanda S Satapathy
DEVCOM Army Research Laboratory

Mary J Graham
SURVICE Engineering Company

REPORT DOCUMENTATION PAGE

Form Approved
OMB No. 0704-0188

1. REPORT DATE *(DD-MM-YYYY)*	2. REPORT TYPE	3. DATES COVERED (From - To)
September 2022	Technical Report	September 2018–May 2019

4. TITLE AND SUBTITLE
Modeling the Rebound of Ballistic Roma Plastilina No. 1 Clay

5a. CONTRACT NUMBER

5b. GRANT NUMBER

5c. PROGRAM ELEMENT NUMBER

6. AUTHOR(S)
Timothy G Zhang, Mary J Graham, and Sikhanda S Satapathy

5d. PROJECT NUMBER

5e. TASK NUMBER

5f. WORK UNIT NUMBER

7. PERFORMING ORGANIZATION NAME(S) AND ADDRESS(ES)
DEVCOM Army Research Laboratory
ATTN: FCDD-RLW-TB
Aberdeen Proving Ground, MD 21005

8. PERFORMING ORGANIZATION REPORT NUMBER
ARL-TR-9540

9. SPONSORING/MONITORING AGENCY NAME(S) AND ADDRESS(ES)

10. SPONSOR/MONITOR'S ACRONYM(S)

11. SPONSOR/MONITOR'S REPORT NUMBER(S)

12. DISTRIBUTION/AVAILABILITY STATEMENT
Approved for public release: distribution unlimited.

13. SUPPLEMENTARY NOTES
ORCID IDs: Timothy Zhang, 0000-0003-4440-6275, Sikhanda S Satapathy, 0000-0003-2694-8740

14. ABSTRACT
Accurate modeling of ballistic Roma Plastilina No.1 (RP #1) clay is very critical to understanding the load transfer between the armor and the clay. Our previous developed model for the RP #1 clay did not account for the rebound due to the limited test data used for the model development. In this study, additional dynamic impact experiments were conducted to provide test data to characterize the rebound. The experiments showed that the rebound depended on the impact velocity and could be as high as 15%. The material model for the RP #1 clay was recalibrated to account for the rebound.

15. SUBJECT TERMS
Sciences of Extreme Materials, Roma Plastilina No. 1 clay, indent, material model, rebound, impact test

16. SECURITY CLASSIFICATION OF:			17. LIMITATION OF ABSTRACT	18. NUMBER OF PAGES	19a. NAME OF RESPONSIBLE PERSON
a. REPORT	b. ABSTRACT	c. THIS PAGE			Timothy G Zhang
Unclassified	Unclassified	Unclassified	UU	37	19b. TELEPHONE NUMBER (Include area code) (410) 306-2984

Standard Form 298 (Rev. 8/98)
Prescribed by ANSI Std. Z39.18

Contents

List of Figures

List of Tables

1. Introduction

Current personal protective equipment (PPE) has drastically reduced battlefield fatalities by using high-performance materials to effectively defeat common threats. Even when the projectile is stopped by the armor, injury can still be sustained due to load transfer to the body from the deforming back face of the armor. One approach to reduce battlefield injuries is to further optimize the performance of PPE; however, this optimization is limited by our understanding of the load transfer to the human body and its response. Currently, deformation into backing is used to assess the injury potential of the threat–armor interaction.

Ballistic Roma Plastilina No. 1 (RP #1) clay is commonly used as the backing material in PPE testing. However, mechanical properties of RP #1 clay depend on strain rate, temperature, and moisture. The material properties for RP #1 clay, including the Young's modulus and flow stress at strain rate of 10^4/s were obtained by a combination of ballistic penetration tests and engineering models and reported in Carton et al. (2014). The flow stress was reported to be 7 MPa at room temperature and 44 °C, which decreased to 1 MPa at 60 °C (Carton et al. 2014). The Johnson-Cook model, $\sigma = 65 + 210\varepsilon^{0.6}(kPa)$ was used in Callahan (2011) to model quasi-static response. Similarly, the Johnson-Cook model was calibrated in Mates et al. (2014) with the following parameters,

$$\sigma = (0.01 + 238\varepsilon^{0.29})\left(1 + 0.25\ln\left(\frac{\dot{\varepsilon}}{0.118}\right)\right)\left(1 - \left(\frac{T - T_0}{T_m - T_0}\right)^{0.502}\right)(kPa)$$

Power law plasticity material model was assumed for RP #1 clay in Hernandez et al. (2015), where the material parameters were obtained by using an indirect method to match drop test data. The fitted material model was reported as $\sigma = 202\varepsilon^{0.101}\left(\frac{\dot{\varepsilon}}{\dot{\varepsilon}_0}\right)^{0.01}(kPa)$. A simplified Cowper-Symonds model was used to model the clay response at high strain rates up to 18,000/s in Buchely et al. (2016). The material parameters were calibrated to match the dynamic indentation test data using a reverse method.

Analytical models were proposed for the depth of penetration (DOP) in the RP #1 clay using spherical cavity expansion theory (Buchely et al. 2016) and the material parameters were determined by matching the dynamic indentation test data. Two analytical models (Li et al. 2019), including compressible and incompressible, were developed for RP #1 clay to predict the DOP accounting for strain hardening, strain rate, and temperature. Dynamic spherical cavity expansion model (Li et al. 2019) was applied to the clay, which was modeled on the Johnson-Cook model. Analytical models were fast running and suitable for parametric study. However,

analytical models usually involved very complex derivation, and the models must be rederived for a different projectile. Another limitation is that analytic models required an analytic material model, which were usually obtained by fitting test data. Semi-infinite geometry was usually assumed for analytic models; that is, boundary conditions were not accounted for.

However, the clay is typically weaker under tension (Laible 1980). In our previous work (Zhang et al. 2017), a clay model with different responses under tension and compression was calibrated for RP #1 clay. The stress-strain curves under compression were obtained from the compression test at a very low rate (~ 0.01/s). The tensile properties and strain rate scaling factors were obtained from sensitivity analysis to best match the impact and drop test data at medium strain rates (~100 /s to ~ 1000 /s). However, only the residual clay indents were measured in the drop tests, and the time history of clay indents did not show the rebound for impact velocity of 55 m/s. Since the limited test data did not show clay rebound, the calibrated model did not account for rebound.

In Mates et al. (2014), the ball was observed to rebound about 25% in the Digital Image Correlation (DIC) measurement of ball movement when it was impacting a clay block. The clay had the same movement of the ball assuming no gap between the clay and ball. Clay rebound was also reported in van der Jagt-Deutekom et al. (2012) when the RP #1 clay was backing hard/soft armor. In Hernandez et al. (2015), drop tests were conducted for RP #1 clay: three sizes (diameters of 63.5, 50.8, and 44.5 mm) of steel sphere dropping from three heights (2.0, 1.5, and 1.0 m). However, the time history of clay indents were only reported up to the peak value and the rebound data were not available.

Due to the existence of rebound, the peak clay indents were larger than the residual clay indents. Usually only the residual clay indents were measured in Chua and Chen (2010) the backing clay; that is, the measurement could not accurately represent the peak transferred force/momentum from the projectiles. X-ray could be used to monitor the dynamic clay indents (van der Jagt-Deutekom et al. 2012), but the clay size was limited to a diameter of 152.4 mm (6 inches), which was much smaller than the standard size of 609.6- × 609.6-mm (2- × 2-ft) clay block in the ballistic tests (Rafaels et al. 2019).

However, the correlation between the peak and residual clay indents could be obtained by numerical models. A material model accounting for rebound was very critical to model the clay. In this report, the work in Zhang et al. (2017) was extended for this purpose. First, the clay model in Zhang et al. (2017) was reviewed. The same material model for the clay was used, but the material parameters were recalibrated with additional test data, which included the clay rebound data. In the

additional ballistic tests, high-speed cameras were used to record the motion of the projectiles to obtain the time history of the clay indents for the drop tests when 1-kg hemispherical nose cylindrical projectiles, dropping from a height of 2 m, impacted the clay block. For the impact tests, the impact velocities were varied (from ~15 m/s, having similar impact energies as the drop tests, to the highest velocity that the projectile can have ~75 m/s) to understand whether the clay rebounded at other impact conditions and quantify the rebound if any. Then a sensitivity study was conducted for both the drop test and impact test and one set of material parameters was obtained for the clay model accounting for the rebound. To the best knowledge of the authors, this was the first time including the rebound in modeling the clay response.

2. Review of Current Clay Model

A US Army Combat Capabilities Development Command (DEVCOM) Army Research Laboratory (ARL) clay model was developed previously based on a series of experiments (Zhang et al. 2017). The compression experiments at low strain rates were conducted to characterize the mechanical properties of RP #1 clay under quasi-static conditions. The experiments were conducted at four different temperatures and three different strain rates. Impact and drop tests were then carried out to characterize the dynamic response at medium strain rates. The drop tests were the calibration process for the clay prior to the impact tests. The residual clay indents in the drop tests were required to be within 25 ± 3 mm so that the impact tests could be conducted on the clay block. In the drop tests, a 1-kg hemispherical nose cylinderical projectile, dropping from a height of 2 m, impacted the clay block. In the impact tests, a 200-g hemispherical nose with long tail projectile impacted the clay block at 55 m/s. The time history of the DOP was recorded in the impact test, while only the residual DOP was measured in the drop tests.

2.1 Compression Tests

Compression tests at various loading rates and temperatures were conducted to characterize the effects of rate and temperature on the clay compressive properties. The clay specimens for the compression tests were fabricated by punching out a 16-mm-diameter sample of 7-mm thickness using a stainless steel mold right before the experiment. Compression tests were performed on a 5985 Universal Testing System (Instron, Norwood, MA), as shown in Fig. 1, which was equipped with an environmentally controlled chamber. The crosshead speeds of 0.05, 0.5, and 5 mm/s were used, with the corresponding nominal strain rates being about 0.007, 0.07, and 0.7 /s. Corn starch was used as a solid-state lubricant to reduce friction between the platen and sample similar to earlier tests of plasticines (Chijiiwa et al.

1981; Sofuoglu and Rasty 2000). The cylindrical samples were held at temperatures of 5, 10, 22, and 38 °C within the environmentally controlled chamber prior to testing for at least 30 min to achieve thermal equilibrium. Tests were recorded using the built-in Instron AVE 2 Extensometer accessory to provide a visual measurement of the strain to ensure its uniformity and, hence, validity of the tests. The top platen was placed 0.5, 5, or 50 mm above the sample at the start of the test to provide a 10 s delay before making contact with the specimen, which allowed adequate time to reach the test velocity of 0.05, 0.5, or 5 mm/s, respectively. Compression tests were terminated when the crosshead had compressed the sample specimens to about 50% of the initial height. Compression tests were repeated for a minimum of six different samples.

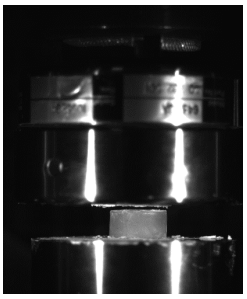

Fig. 1 Compression tests

One tested true stress-strain curve, which usually had the largest strain, was chosen from each test condition and plotted together, as shown in Fig. 2. The stress-strain curves had similar shapes for all the temperatures and rates. As the temperature decreased, the stress increased significantly. Similarly, the stress increased as the loading rate increased. Therefore, the clay material properties had strong dependences on temperatures and loading rates.

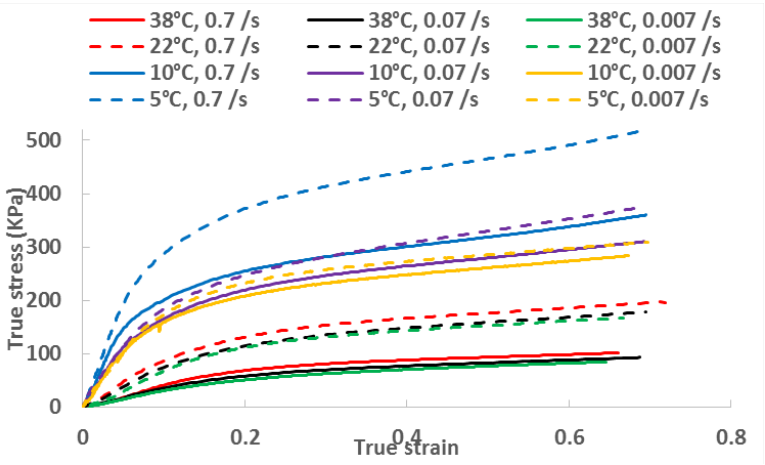

Fig. 2 The true stress-strain curves from the compression tests for the clay

2.2 Impact Tests

In the original impact tests conducted by Prather et al. (1977), the DOP in the clay was still increasing at the end of data collection. The impact experiments were repeated in Ivancik et al. (2017) to obtain longer time history of penetration depth in the clay so that the maximum DOP and rebound, if any, could be captured.

Figure 3 shows the test setup. Cameras were used to capture the movement of the projectile tail so that the DOP could be measured assuming no gap between the projectile tip and the clay. The projectile had a long tail so that the tail end could be tracked by the camera during the impact. The impact side of the clay block was 304.8 × 304.8 mm in dimension. The block was 279.4 mm thick. The clay block rested on a metal frame. The projectile was an 80-mm-diameter hemispherical-nosed cylinder with a 12.4-mm diameter and 167-mm-long tail. The projectile materials were Nylon 101 and Delrin for the hemispherical head and the cylindrical tail, respectively. The mass of the projectile was 200 g, which was the same as that used by Prather et al. (1977). The impact velocity was approximately 55 m/s for all 20 tests.

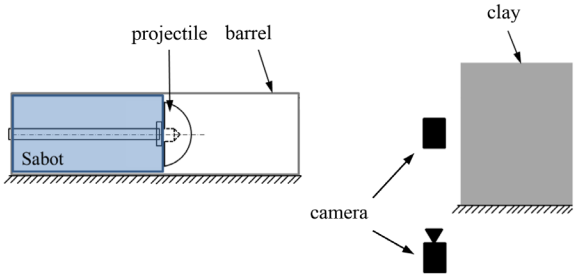

Fig. 3 Impact test setup

Figure 4 shows the time histories of DOP for all 20 tests. The clay temperatures were between 33 °C and 37 °C for the tests. As the projectile penetrated into the clay, it slowed down, and hence the slope decreased. The DOP reached the peak around 5 ms and remained nearly constant after that. The peak DOP for the tests were between 89 and 104 mm, with an average of 96.7 mm. The two curves corresponding to the highest and lowest DOP were used to represent the test data range, and were used later for comparison with numerical results. The original test data from Prather et al. (1977) was also plotted for comparison. The DOP from Prather et al. was only recorded for less than 3 ms and it was still rising. The DOP in Prather's test increased slightly faster compared to the measurements in the repeat tests, indicating that the clays in the two different tests possessed different material properties due to different processing process and environment conditions.

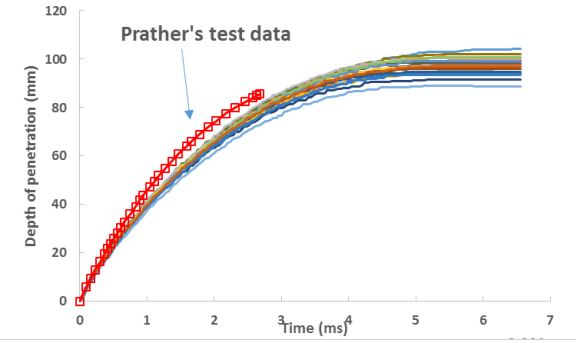

Fig. 4 The time histories of DOPs for 20 impact tests; the test data from Prather et al. (1977) was also included for comparisons

2.3 Drop Tests

Prior to the impact tests, each clay block was calibrated using the column drop calibration test standard (ATC 2008) as shown in Fig. 5a. The clay block was contained by half-inch aluminum frames (at the sides) with top and bottom unconfined. Two thermocouples were placed 2 inches deep in two opposite corners of the striking face. Three consecutive drops were made within the striking face of the clay block. The edge of each dimple created by the impact was at least 76.2 mm from the edge. The distances between impact dimple centers was at least 76.2 mm. The material consistency required that a depression of 25 ± 3 mm in depth was obtained when a 1.0 kg ± 10-g cylindrical steel mass of 44.5 ± 0.5-mm diameter having a hemispherical striking end, was dropped from a height of 2.0 m ± 2 cm onto the flat material striking surface. The impactor was removed to measure the residual clay indent. If the clay passed the drop tests, the striking face was then repaired and smoothed over where applicable prior to the impact tests.

Figure 5b shows the residual DOP results for 60 drop tests. The DOP varied between 24 and 28 mm. The average value of the DOP was about 26.6 mm. All of these 60 DOP measurements were between 22 and 28 mm and met the criterion for the impact tests.

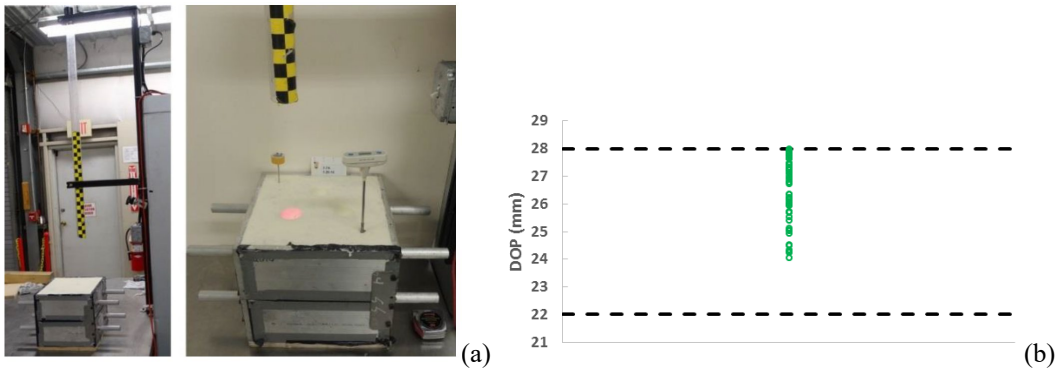

Fig. 5 Drop test (a) setup, and (b) results

A material model was calibrated based on the experimental data. The compression test results were used as the material stress-strain curves at quasi-static conditions. A parametric study was conducted to obtain one set of material parameters to best fit the drop and impact test data. Only the residual clay indents were measured in the drop test data, and the time history of DOP did not show remarkable clay indents for 55 m/s impact tests. The material model calibrated based on the available test data did not account for rebound.

2.4 Material Model

Commercial software LS-DYNA was used to model the clay impact and drop tests. *MAT_PLASTICITY_COMPRESSION_TENSION (LSTC 2016) was selected as the material model for the clay (Zhang et al. 2017). This is an isotropic elastic-plastic material with different yield stress versus strain responses under compression and tension. The material is eroded when the plastic strain exceeds a prescribed value. Previous low rate compression tests showed that the clay response was rate and temperature sensitive. The material model was assumed to follow $\sigma(\varepsilon, \dot{\varepsilon}, T) = \alpha_{\dot{\varepsilon}}(\dot{\varepsilon})\alpha_T(T)f(\varepsilon)$. Function $f(\varepsilon)$ represented the baseline stress-strain curve at quasi-static conditions. The effect of strain rate was modeled by scaling the baseline stress-strain curve by factor $\alpha_{\dot{\varepsilon}}(\dot{\varepsilon})$. The effect of temperature was also included with scaling factor $\alpha_T(T)$.

The clay model was characterized based on drop and impact tests, and the details can be found in Zhang et al. (2017). Figure 6a shows the baseline stress-strain curve for the model including both compression and tension phases. The compression stress-strain curve was taken from the compression tests at 38 °C at a rate of 0.007/s. The stress-strain curves at lowest strain rate were selected since they were the closest data to quasi-static conditions. The tensile stress-strain curve was not measured experimentally, but was calibrated to match the drop and impact test data. The tensile stress-strain curve was linear up to 15 kPa and then remained constant,

and was designated as (15, 15); the first number was the stress value transit between two linear curves, while the second number was the tensile stress value at strain of 1. The strain rate scaling factor was shown in Fig. 6b as a function of strain rates. The same strain rate scaling factors were applied to both compression and tension responses. The average temperature in the clay for the drop and impact tests was 35 °C, but the stress-strain curve at 38 °C was used for the model. Assuming that the properties varied linearly with temperature, the property of 35 °C would be 20% higher than that of 38 °C; that is, the temperature function $\alpha_T(T)$ was 1.2 for the clay in the drop and impact tests under the test standard (ATC 2008). For this material model, however, the temperature is not calculated for the clay. Therefore, the temperature term $\alpha_T(T)$ was predetermined depending on the temperature of the tested clay. This assumption could cause some inaccuracy in predicting the clay response under impact when the clay temperature in the impact zone could change and the material response strongly depended on the temperature. The objective of this work was to calibrate a material model for clay, which matched well with the test data; that is, the effect of temperature was implicitly included in the material parameters. The friction coefficient was 0.193 (Hernandez et al. 2015). For the clay model *MAT_PLASTICITY_COMPRESSION_TENSION, both compressive and tensile Young's modulus were required in the material card. 15 MPa was used for both the Young's modulus under compression and tension.

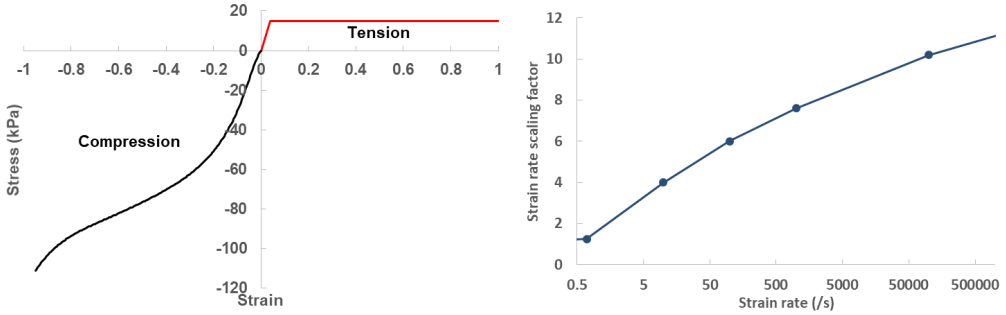

(a) (b)

Fig. 6 The clay material model: (a) baseline stress-strain curve $f(\varepsilon)$, (b) strain-rate scaling factor $\alpha_{\dot{\varepsilon}}(\dot{\varepsilon})$

Table 1 lists the calibrated material parameters for the clay model without rebound. Both the compressive and tensile Young's modulus were 15 MPa. The compressive stress-strain curve was taken from the compression test at a strain rate of 0.007/s and temperature of 38°C. Both the tensile stress-strain curve and rate scaling factor were obtained from the parametric study. The tensile stress-strain curve was linear up to 15 kPa and then remained constant. This set of material parameters were not unique.

Table 1 Characterized parameters of clay model without rebound for RP #1 clay

Young's modulus (MPa)		Stress-strain curve		Strain rate scaling factor $\alpha_{\dot{\varepsilon}}(\dot{\varepsilon})$
Compressive	Tensile	Compressive	Tensile	
15	15	Fig. 6a	(15, 15), Fig. 6a	Fig. 6b

Figure 7 shows the Finite Element model for the drop test. A 1 kg hemispherical-nosed cylindrical steel projectile impacted the clay block at 6.1 m/s, which was equivalent to a drop from a height of 2 m (the distance between the clay impact surface and projectile rear face was 2 m, the actual drop height was 1.91 m after subtracting the projectile length). A quarter symmetry model was used to take advantage of the symmetry. A finer mesh was used in the impact zone to better capture the interaction between the projectile and the clay. The frame and the plywood used to hold the clay block were not modeled. Instead, the bottom surface of the clay was constrained in normal direction to represent the plywood. The friction effects between the clay and frames/plywood were not included in this study.

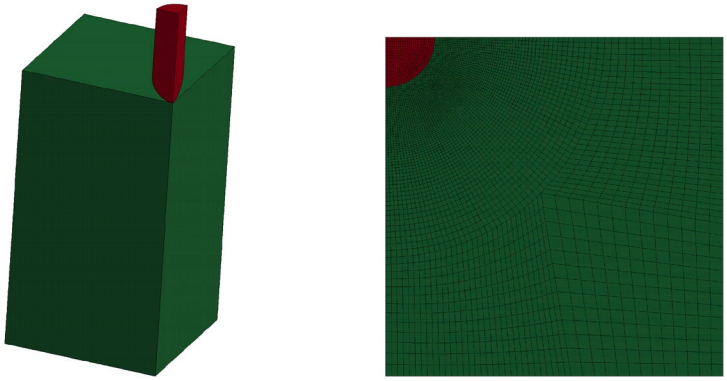

Fig. 7 Drop test model

Figure 8 shows the Finite Element model for the impact tests. A 200-g hemispherical-nosed projectile impacted the clay block. The Nylon 101 hemispherical nose and the Delrin cylindrical tail were both modeled, and they share nodes at their interface. Elastic material models were used for both Nylon 101 and Delrin. The density, Young's modulus, and Poisson's ratio were 1203 Kg/m^3, 2.93 GPa, 0.39, and 1486 Kg/m^3, 2.41 GPa, 0.35, for Nylon and Delrin, respectively. The impact tests were not symmetrical since the clay block rested on a metal frame during the test. As an approximation, a quarter symmetry model was still used with normal displacement constrained to zero on one side to represent the metal frame.

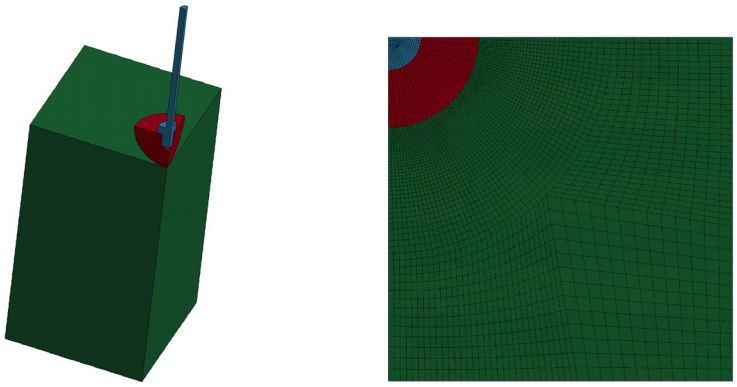

Fig. 8 Impact test model

Figure 9 shows the comparisons between the current clay model predictions and the test data for both drop and impact tests. "Min" and "Max" denote the minimum and maximum test data to bracket out the test variations. The calibrated clay model did not account for the clay rebound due to the available test data.

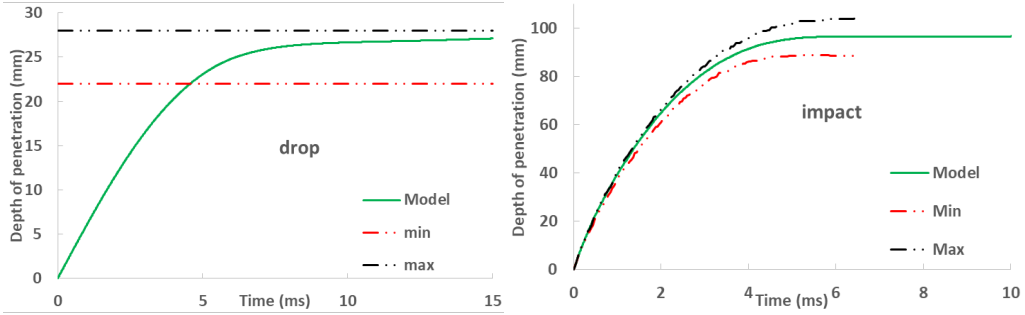

(a) (b)

Fig. 9 Comparisons between current clay model predictions and test results for (a) drop tests, and (b) impact tests

In Mates et al. (2014), the ball was observed to rebound about 25% in the DIC measurement of ball movement when it was impacting a clay block. The clay was assumed to have the same movement as the ball if there was no gap between the clay and ball. If rebound exists for the clay, the model needs to be updated to account for it; otherwise the clay model would underestimate the clay peak indents.

3. Recalibrated Clay Model

Additional ballistic impacts, including drop tests and impact test, were conducted at DEVCOM Army Research Laboratory to characterize whether rebound existed for the clay. Only the time history of clay movements could provide rebound data. To achieve this, high-speed cameras were used to record the time history of clay deformation for the drop tests instead of only measuring the residual indents. For

the impact tests, the impact velocities were varied to explore whether clay rebounded at other velocities.

3.1 Experiments

Twelve additional drop tests were performed to explore the clay rebound. All of the residual indentations were measured in the clay with a caliper after removing the impactor. To capture the dynamic clay indent, the projectile tail motion was captured with a Phantom high-speed camera at 20,000 frames per second (fps). Assuming there was no gap between the projectile tip and the clay, the evolutions of the clay deformation including rebound were obtained. The temperature of the clay was also measured before the tests.

3.1.1 Drop Tests

Prior to the impact experiments, the RP #1 clay in the rectangular box, including aluminum frame, and PVC were conditioned in a temperature-controlled environment to ensure passing the indentation depth requirement. The clay was packed and conditioned by a pneumatic to remove voids. When the target was removed from the temperature-controlled environment and placed in the testing area, gauges were placed in the clay. The experiment was performed when the temperature reached a range of degrees to avoid, as much as possible, the influence of excessive heating.

Table 2 contains all of the data collected from all 12 drop tests, including rectangular box (there were two different aluminum encased RP #1 blocks used), rectangular box face for the drop (top and bottom), and temperature in the sample, and residual DOP. The impactor was aimed at the clay surface center. The clay indents must be within 22 to 28 mm to meet the requirements so that the impact tests can be conducted on the clay. For drop tests 2, 6, 7, and 11, the final clay depths were less than 22 mm, so the clay from these four tests did not meet the requirements and could not be used for the impact tests. However, these four tests still provided the time history of dynamic clay indents, which could be used to understand whether the clay rebounded after reaching its peak value; therefore, these four tests were not excluded in this study.

Table 2 The clay temperature and residual indents in new drop test data

Drop #	Target	Face	Temperature (°F)	Residual indent (mm)
1	Box 1	Top	95.2	24.2
2	Box 1	Bottom	92.8	19.7
3	Box 2	Top	94.7	23.2
4	Box 2	Bottom	92.6	25.0
5	Box 1	Top	92.8	23.4
6	Box 1	Bottom	92.4	18.3
7	Box 2	Top	92.2	20.7
8	Box 2	Bottom	92.5	22.4
9	Box 1	Top	96.3	23.6
10	Box 1	Bottom	96.3	23.1
11	Box 2	Top	95.1	21.0
12	Box 2	Bottom	96.1	24.2

The time history of the DOP from the drop tests were extracted every half a millisecond from the individual frames gathered by the high-speed camera at 20,000 fps using Phantom Camera software (PCC 2.5). Time zero was set right before impact; images were advanced every 10 frames; and distances were measured from the back end of the dropper. Graphs of the extracted time history of the DOP for the drop tests are shown in Fig. 10. All graphs are qualitatively the same; that is, DOP increases rapidly to peak value, rebounds, and stabilizes. The peak clay indents ranged from 25.4 to 32.43 mm. Rebounding occurred at approximately 9 ms until leveling/stabilizing. The percentage of rebound was significant, between 10% to 20%, and cannot be ignored.

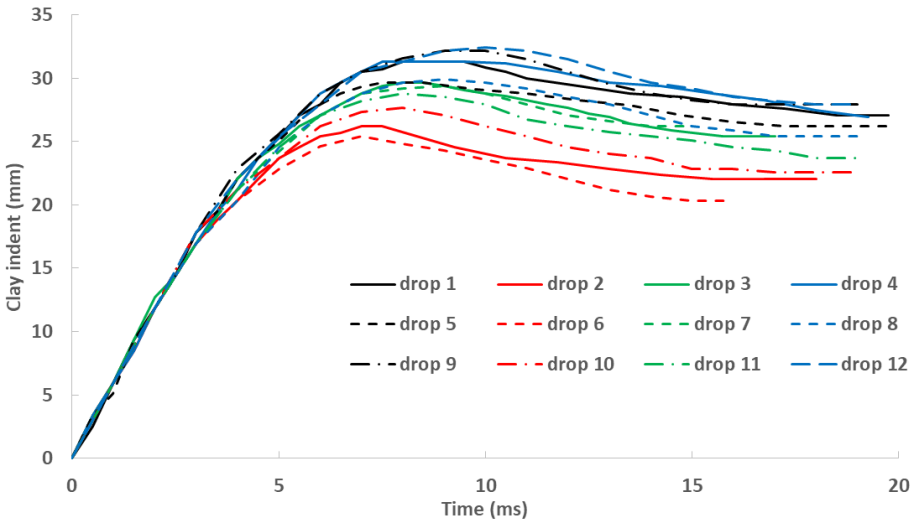

Fig. 10 Time history of DOP for the drop tests

Table 3 shows the residual clay indent measured by the caliper after removing the impactor, the peak indent, and the indent of last frame measured by the high-speed camera. The rebound, difference between peak indent, and indent of last frame measured by high-speed camera were also listed in the table. The rebound percentage, the rebound divided by the peak indents, was about 15% by average. The high-speed camera only recorded the tests up to 20 ms, and the clay indents could continue to drop after the last frame. When the impactor was removed from the clay, the clay deformation could recover. These two factors might explain that the residual indents were 2–6 mm lower than the indents of last frame measured by the high-speed camera, except test 10.

Table 3 The clay rebounds for 12 additional drop tests

Test #	Residual indent (mm)	Peak indent (mm)	Indent of last frame (mm)	Rebound (mm)	Rebound percentage
1	24.2	31.3	27.1	4.2	13.5%
2	19.7	26.3	22.0	4.3	16.1%
3	23.2	29.6	25.4	4.2	14.3%
4	25.0	31.3	26.9	4.4	14.0%
5	23.4	29.6	26.3	3.3	11.4%
6	18.3	25.4	20.3	5.1	20.0%
7	20.7	29.4	26.3	3.1	10.6%
8	22.4	29.9	25.4	4.5	15.0%
9	23.6	32.2	27.9	4.3	13.2%
10	23.1	27.7	22.6	5.1	18.4%
11	21.0	28.8	23.7	5.1	17.7%
12	24.2	32.4	27.9	4.5	13.8%

3.1.2 Impact Tests

Sixteen side-impact tests were performed. The dimensions of the rectangular block were the same as the drop tests, except the aluminum frames were removed prior to impact. Before every impact test, drop tests were performed to calibrate the condition of the RP #1 clay. The residual clay indents need to be within 22 to 28 mm to pass the calibration tests. As shown in Fig. 11, the rectangular clay block was sitting on a metal frame on a table for the impact tests. A 25.4-mm-thick plexiglass plate was against the lower back of the clay block.

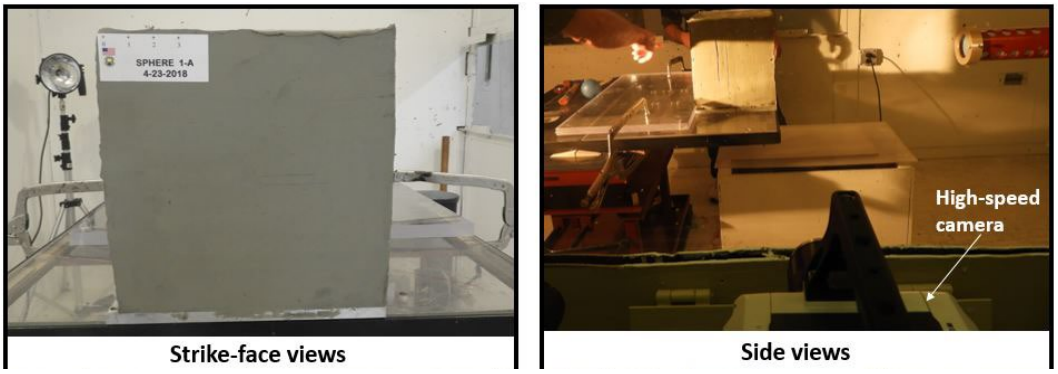

Fig. 11 RP #1 clay block in the impact tests, front view (left) and side view (right)

The evolution of the projectile tail was captured with a Phantom high-speed camera at 30,000 fps. The evolution of the clay indent was assumed to be the same as the projectile if there was no gap between the projectile tip and clay. In the previous tests, the impact velocities were approximately 55 m/s and no rebound was observed from the time history of the clay indents. In this series of tests, the impact velocities were varied to explore whether rebound existed for other impact conditions. Three ranges of velocities were selected, as shown in Table 4. It was already shown that clay rebounded in the low velocity drop tests. To have the same impact energies as the drop tests, the impact velocity was calculated to be approximately 13.7 m/s in the impact tests. This velocity was selected as the low velocity range, larger than 10 m/s and less than 20 m/s. Medium velocity was about twice the low velocity. To determine the high-velocity range, the impact velocity was continued to increase from 55 m/s but ensured that the DOP was up to half of the clay thickness. The impact velocity was up to 76 m/s, which reached the capacity of the gas gun used to launch the projectile. The high velocity was set between 60 and 80 m/s. The test number is also shown in Table 4. Impact 1-A, out of the field of view of the high-speed camera, is not considered in the analysis.

Table 4 Three impact velocity ranges for the impact tests

Low velocity, < 20 m/s	Medium velocity, ~ 30 m/s	High velocity, > 55 m/s
		5-A, 61.9 m/s
		5-B, 61.1 m/s
1-A, 11.2 m/s (No data)	3-A, 30.9 m/s	6-A, 65.2 m/s
1-B, 17.6 m/s	3-B, 30.7 m/s	6-B, 66.0 m/s
2-A, 16.6 m/s	4-A, 29.2 m/s	7-A, 75.1 m/s
2-B, 15.8 m/s	4-B, 32.7 m/s	7-B, 72.8 m/s
		8-A, 76.2 m/s
		8-B, 70.9 m/s

The time history of the DOP was extracted from individual frames gathered by the high-speed camera. Time zero was when the penetration started and data were advanced in increments of 10 frames. Graphs of the extracted time history of the DOP are shown in Fig. 12. There are 15 graphs (Impact 1-A is not included). The curves are qualitatively the same: The DOP increased to its peak value at around 2 ms, rebounded slowly or stabilized.

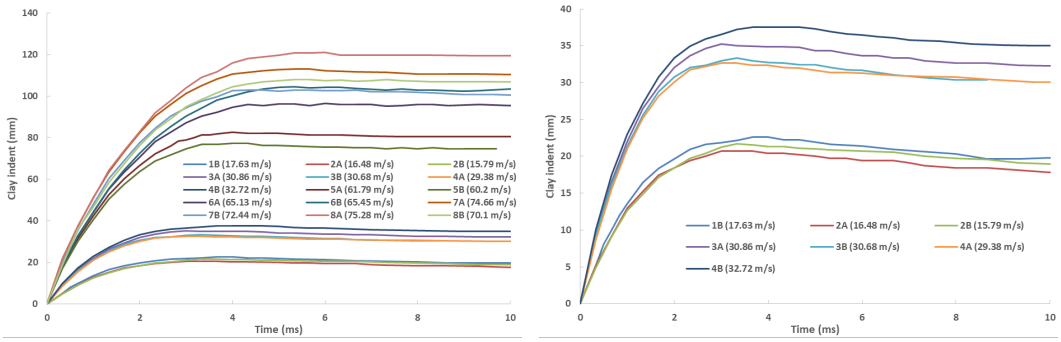

(a) (b)

Fig. 12 The time history of DOP for (a) low, medium, and high velocity, and (b) low and medium velocity

A graph of the peak clay indents versus impact velocity is shown in Fig. 13, along with old tests (the impact velocity was around 55 m/s). The peak clay indents increased with the impact velocity. The peak clay indents in the new tests were lower than the old tests, which might be due to different properties of the RP #1 clay used in the two tests.

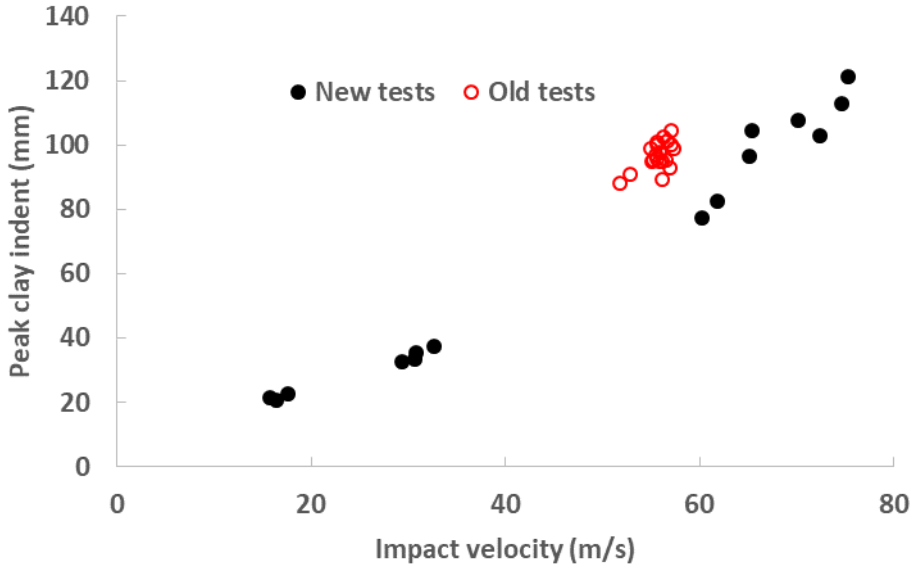

Fig. 13 Peak clay indent versus velocity

The percentages of clay indent rebound versus velocity are shown in Fig. 14 for the 15 impact tests. The percentage of rebound decreased with velocity. When the impact velocity was 60 m/s and higher, the hemispherical section of the impactor penetrated far enough into the block that the clay behind the hemisphere slightly closed to prevent the rebound. Figure 15 shows the clay block with projectile after the impact tests for various velocities. At lower impact velocity, the hemispherical section did not penetrate into the clay and could rebound with less resistance. The rebound percentage was about 15% for low impact velocity (< 20 m/s), which was similar to the rebound percentage in the drop tests.

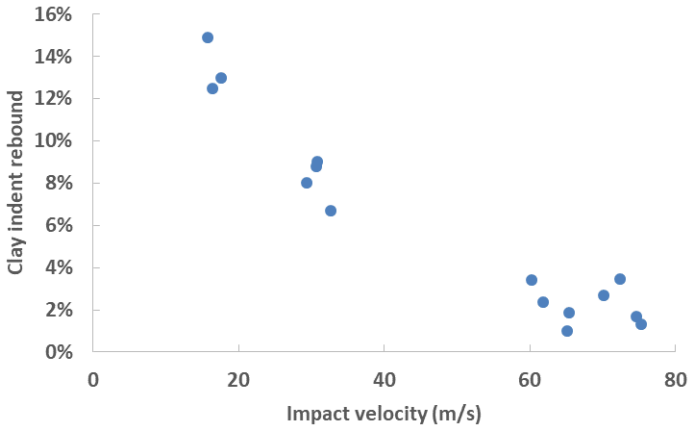

Fig. 14 Percentage of rebound for the impact tests

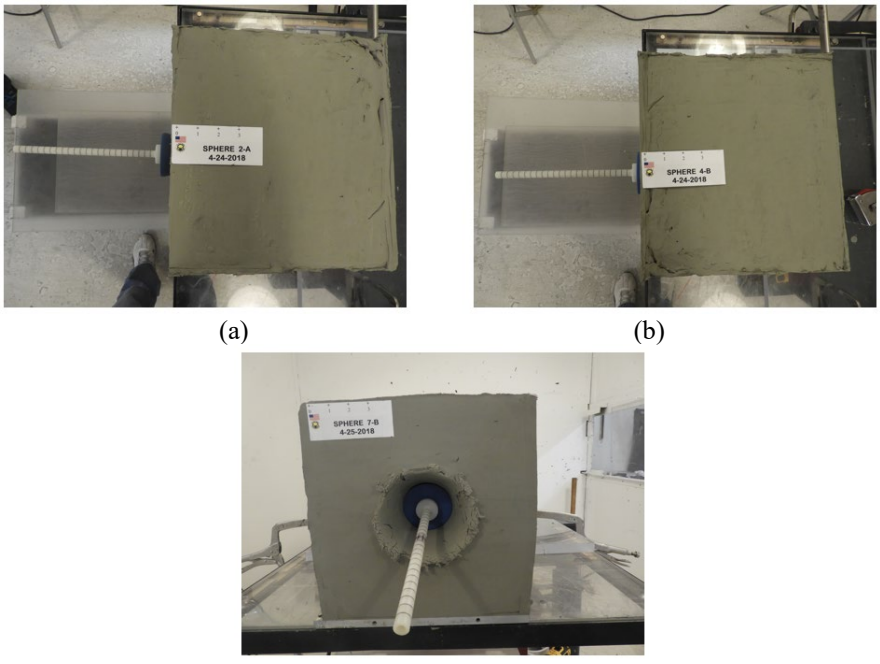

(a) (b)

(c)

Fig. 15 The clay block with projectile after the impact tests for (a) low velocity, (b) medium velocity, and (c) high velocity

The clay rebounded for both drop and impact tests. If only the final clay indents are measured in ballistic experiments, the measurements might not correlate well with the injury. The injury is more likely related to the peak clay indents. It is critical for the clay model to capture the clay peak and rebound. In the following, the material model for the clay was recalibrated. The same material model was used for the clay, but the material parameters were adjusted to capture the rebound.

3.2 Model Recalibration

To capture the clay rebound, the material unloading behavior should be modified so that the residual strain is smaller than the peak strain. In Fig. 16, the clay material was loaded to point A along the compressional stress-strain curve and then it was unloaded. The residual strain depended on the unloading slope, or the Young's modulus. The absolute value of residual strain of unloading curve AC is smaller than that of curve AB, that is, the material rebounded more when it followed the curve AC than curve AB.

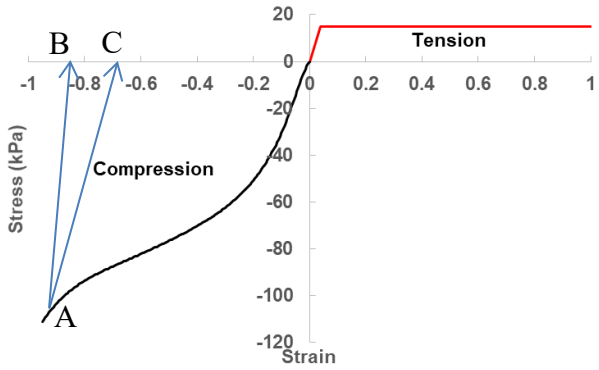

Fig. 16 Unloading of the stress-strain curve

Parametric study in Zhang et al. (2017) showed that the clay indents were mainly dependent on the tensile stress-strain curve and strain rate scaling factor. When the Young's modulus is modified, the clay response will change. The tensile stress-strain curve and strain rate scaling factors might need to be adjusted to match the test data.

3.2.1 Drop Tests

In order to recalibrate the clay model, drop test was selected to do parametric study to understand the effects of the material parameters. Figure 17b shows the pressure time histories at various locations in the impact zone. The impact locations were given in Fig. 17a. "center," "y1," and "y2" were along the impact line, and "X" was in the impact surface. The pressures remained positive for initial 6 ms for locations along the impact line and then dropped close to zero (positive for "X" and negative

for “y1” and “y2”). The pressure at location “X” was negative at a very early time, but then remains positive. Overall, the pressures in the impact zone were mainly positive and sometimes under negative pressure but with small magnitude. This indicates that the parameters related to tensile response—for example, the tensile stress-strain curve—should have minor effects.

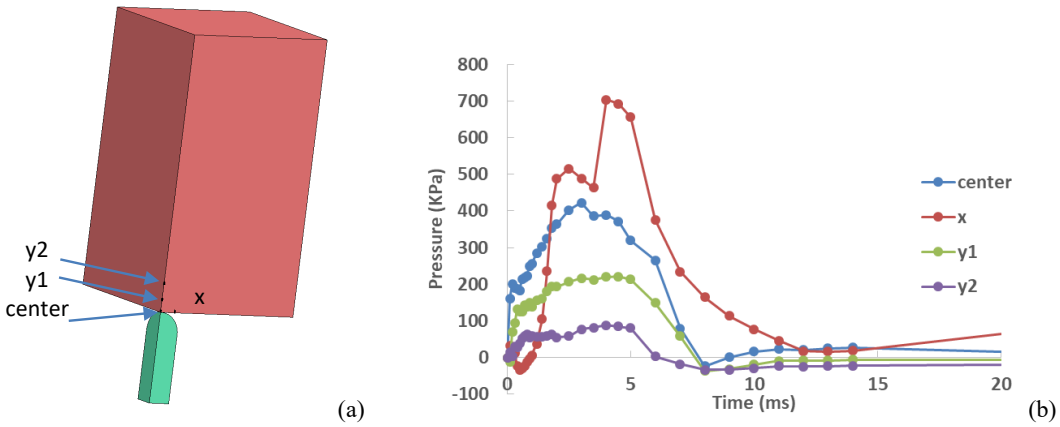

Fig. 17 (a) The locations, and (b) the pressure time history for typical locations in the impact zone

Figure 18b shows the time histories of clay indent for various tensile stress-strain curves given in Fig. 18a. It can be seen that the tensile stress-strain curves almost had no effects on the clay indent until the peak. Overall, the effects of tensile stress-strain curves had minor effects on the clay response. Therefore, the tensile stress-strain curve (15, 15) was still used in the remaining calculations unless specified. The effects of tensile stress-strain curves will be further studied in the impact tests.

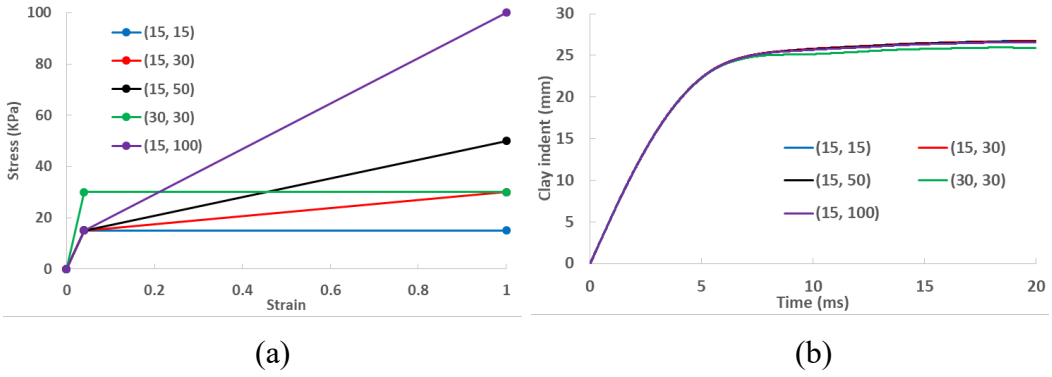

Fig. 18 (a) Various tensile stress-strain curves, and (b) the corresponding clay indent time histories

Figure 19 shows the time history of clay indent for various compressive Young’s modulus E_c (tensile Young’s modulus was fixed at 15 MPa). As the compressive Young’s modulus increased, the clay indent decreased as expected. As the clay

became stiffer, it took less time to reach the peak indent. When the compressive Young's modulus was between 1 MPa and 5 MPa, the peak clay indent was within the "Max" and "Min" test data. As the compressive Young's modulus E_c decreased, for example, 1 MPa and 0.6 MPa, the clay indent rebounded a small amount after the peak.

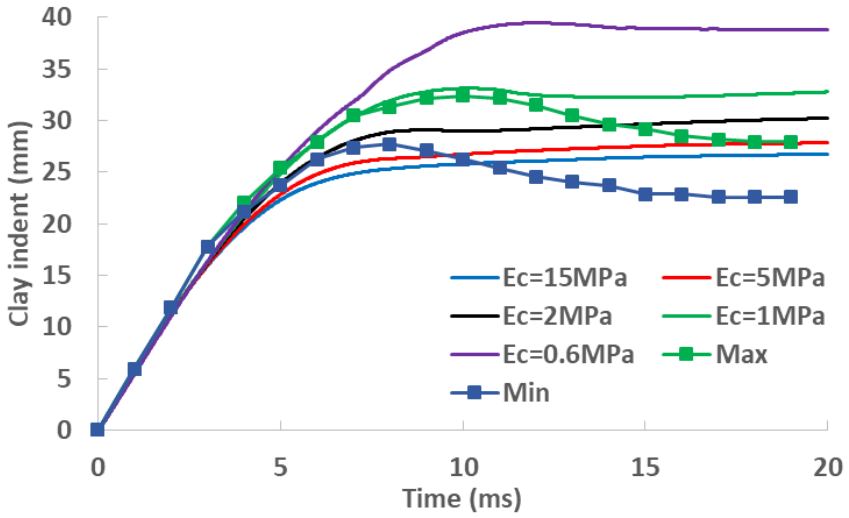

Fig. 19 The time histories of clay indent for various compressive Young's modulus (tensile Young's modulus was fixed at 15 MPa)

Figure 20a shows the effects of tensile Young's modulus E_t on the clay indents. Five tensile Young's moduli E_t, 15, 5, 2, 1, and 0.5 MPa were selected. The tensile moduli almost had no effects on the clay indents up to the peak. As the tensile modulus decreased, the magnitude of rebound increased. The clay indent was within "Max" and "Min" test data, and the rebound was similar to the test data when the compressive and tensile moduli were E_c = 2 MPa and E_t = 1 MPa, respectively. The Young's modulus agreed with the Young's modulus value of 1.7 MPa in Buchely et al. (2016). Obviously, the compressive and tensile Young's modulus can be optimized using least square method.

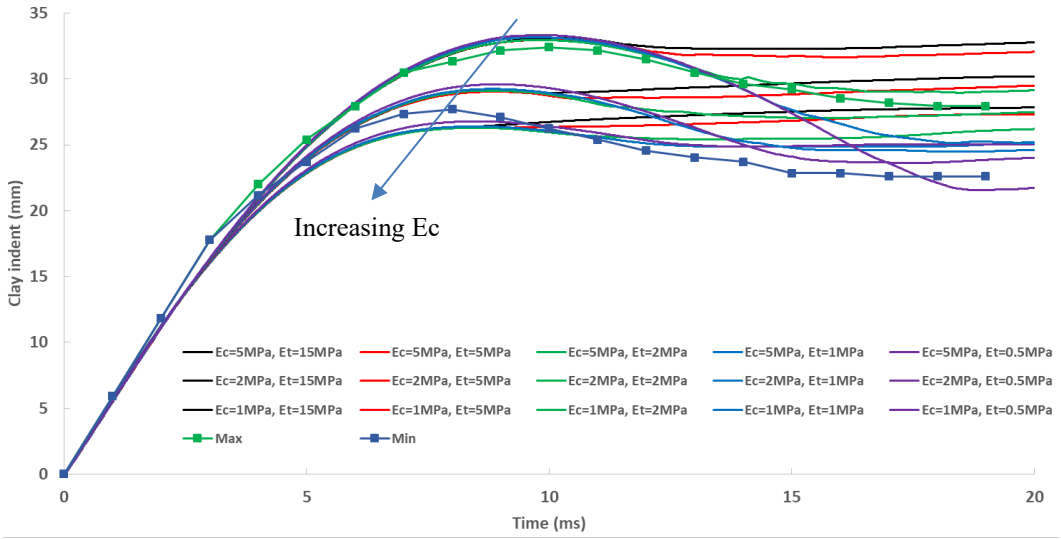

Fig. 20 Effect of tensile Young's modulus on the clay responses

Figure 21 shows the time histories of the clay indent for various tensile stress-strain curves for E_c= 2 and E_t=1 MPa, when the clay rebound was captured. The tensile stress-stain curves almost had no effects on the peak clay indent, but had small effects on the rebound.

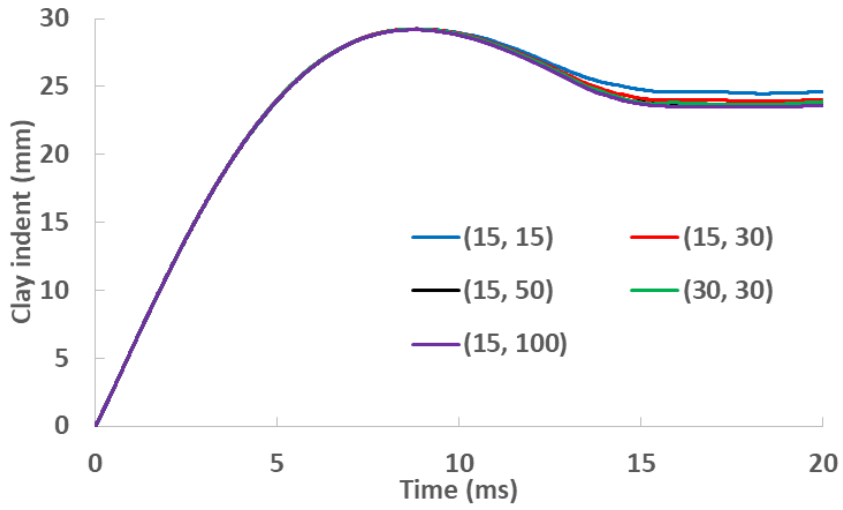

Fig. 21 Effect of the tensile stress-strain curves on the clay indent time histories (E_c= 2 and E_t=1 MPa)

Figure 22b shows the time histories of clay indent for various strain rate scaling factor curves in Fig. 22a. Curve baseline was the strain rate scaling factor curve used in the clay model without rebound. The scaling factor was 1 when the strain rate was 0.007/s and lower (the stress-strain curve used in the material model was corresponding to a strain rate of 0.007/s). The strain rate factors were 1.1 and 1.3 for strain rates of 0.07 and 0.7/s, calculated from the stress-strain curves from the

compression test. Only the strain rates above 0.7/s were varied. Curve baseline, curve A, and curve D followed the same curves until 100/s, curve B and curve C followed the same curves with the baseline until 10/s, and curve E started to be different from curve baseline at 1/s. For curve B, the strain rate factor was fixed at 7 when the rate was higher than 100/s. In Buchely et al. (2016), it was shown that the Young's modulus increased from 1.7 MPa at quasi-static to 11.6 MPa at a rate of approximately 2000/s, which is about 7 times increase. Curve B was included here to match the results in Buchely at al.

The clay indents were almost identical for baseline, curve A and curve D, indicating that the strain rate scaling factors for a rate greater than 100/s had negligible effects. Curve B and C gave slightly different clay indents, so the strain rate scaling factors for a rate between 10 and 100 had small effects, while the rate scaling factors between 1 and 10/s had the most effects based on the results for curve E.

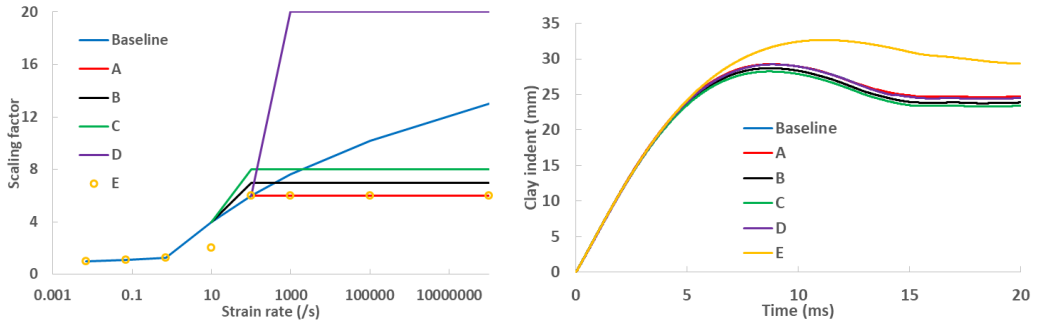

(a) (b)

Fig. 22 (a) Various strain rate scaling factor curves, and (b) the corresponding clay indent time histories

The parametric study of the drop tests showed that the tensile stress-strain curve had negligible effects on the clay indents, but the compressive Young's modulus determined the peak indents and the tensile Young's modulus determined the rebounds. A set of the compressive and tensile Young's modulus were obtained from the parametric study by matching the test data. This set of modulus might not be unique. The parametric study also showed that the strain rate scaling factors had very small effects on the clay indent when the strain rates were larger than 10/s. The tensile stress-strain curve and strain rate scaling factors were not determined from the drop tests. The next parametric study will be conducted on the impact tests to determine a set of the remaining two parameters.

3.2.2 Impact Tests

In the drop test models, the tensile stress-strain curves had minor effects on the clay indents. The same parametric study was conducted for the impact test models for

three impact velocities: 16, 31, and 55 m/s. Figure 23 shows the time histories of clay indent for five different tensile stress-strain curves given in Fig. 18a. It can be seen that the effects of tensile stress-strain curves could not be ignored for all the three impact velocities. As the tensile yield stress increased, the clay indent dropped. At 55 m/s, the calculations crashed for (15, 100) case. The model predictions were within the experimental data only for the tensile stress-strain curve (15, 50). Therefore, the tensile stress-strain curve (15, 50) will be used in the material model.

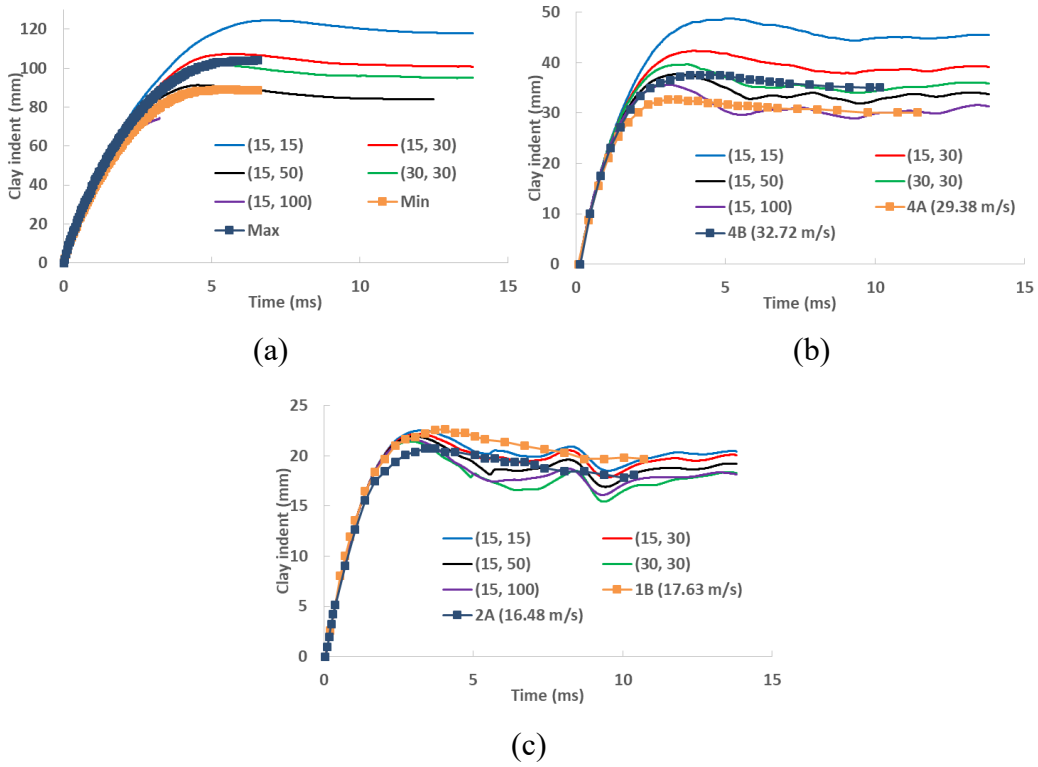

Fig. 23 The effects of tensile stress-strain curves for impact velocity of (a) 55 m/s, (b) 31 m/s, and (c) 16 m/s

Figure 24 shows the effects of strain rate scaling factors on the clay indents. The strain rate scaling factor curves were the same as given in Fig. 22a. It can be seen that only the results agreed with the test data for curve baseline and curve B, and the difference was small between curve baseline and curve B, indicating that the strain rate scaling factor for strain rates higher than 600/s has minor effects on the clay indents in the impact tests at 55 m/s and lower impact velocities. So curve B is selected as the strain rate scaling factor curve for the material model. Curve B was chosen to match the material stiffening from quasi-static to dynamic conditions in Buchely et al. (2016). Therefore, curve B was reasonable.

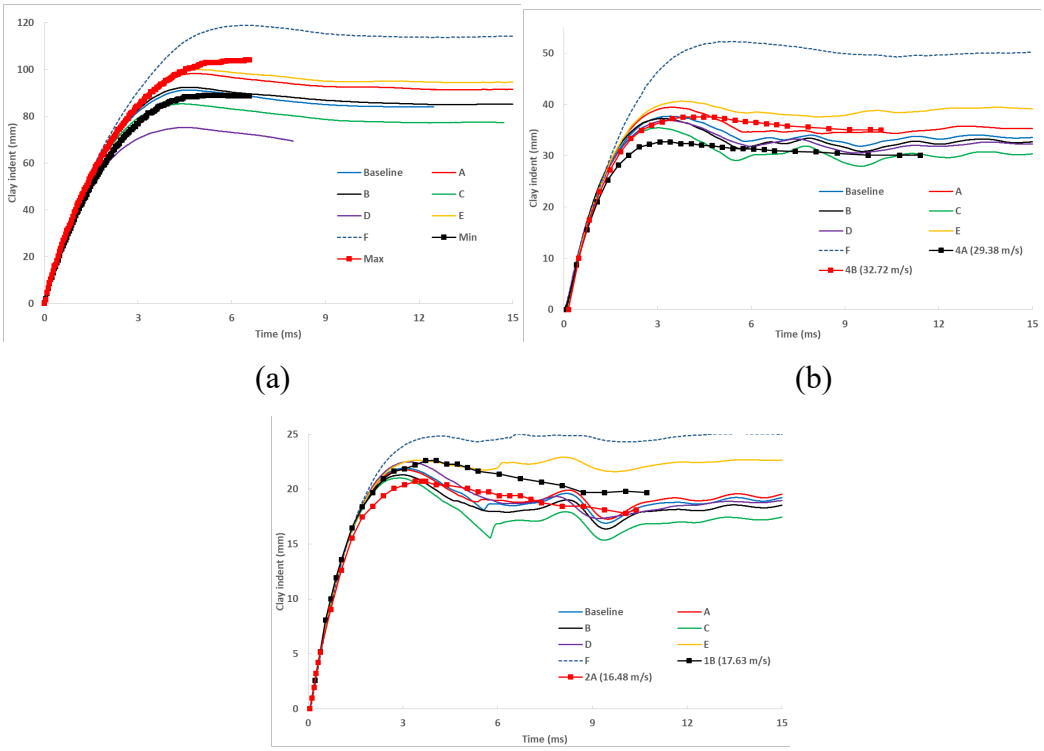

Fig. 24 The effects of strain rate scaling factors on the clay indents for impact velocity of (a) 55 m/s, (b) 32 m/s, and (c) 16 m/s

A set of material parameters were determined for the clay model to best match the test data. This set of material parameters might not be unique. The comparison between the recalibrated model and current model was summarized in Table 5. The Young's modulus were updated to capture the clay rebound. The compressive Young's modulus dominates the peak clay indents while the tensile Young's modulus dominates the magnitude of rebounds.

Table 5 Characterized parameters for RP #1 clay

Model	Young's modulus (MPa)		Tensile stress-strain curve	Strain rate scaling factor $\alpha_{\dot{\varepsilon}}(\dot{\varepsilon})$
	Tensile	Compressive		
Current without rebound	15	15	(15, 15)	Dashed line in Fig. 25
Recalibrated with rebound	1	2	(15, 50)	

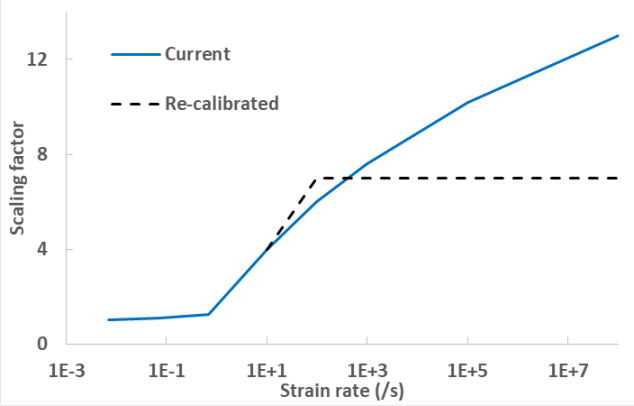

Fig. 25 The recalibrated strain rate scaling factors

The recalibrated clay model was used to model the drop tests and impact tests of three velocities. The comparisons between models and experimental results are shown in Figs. 26 and 27 for drop tests and impact tests, respectively. The clay model captured the response very well including the peak and rebound observed in the drop tests. For the impact tests, four velocities were included, low, medium, and high velocity, used in the experiments, and 55 m/s, used in previous impact tests. The model had reasonable agreements of the peak indents and magnitude of rebound with the impact tests for different velocities; however, the clay rebounded faster in the model, that is, it took less time for the clay to rebound.

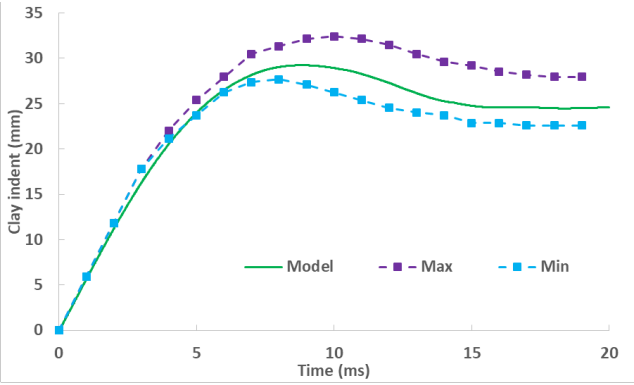

Fig. 26 Comparison between models and drop tests

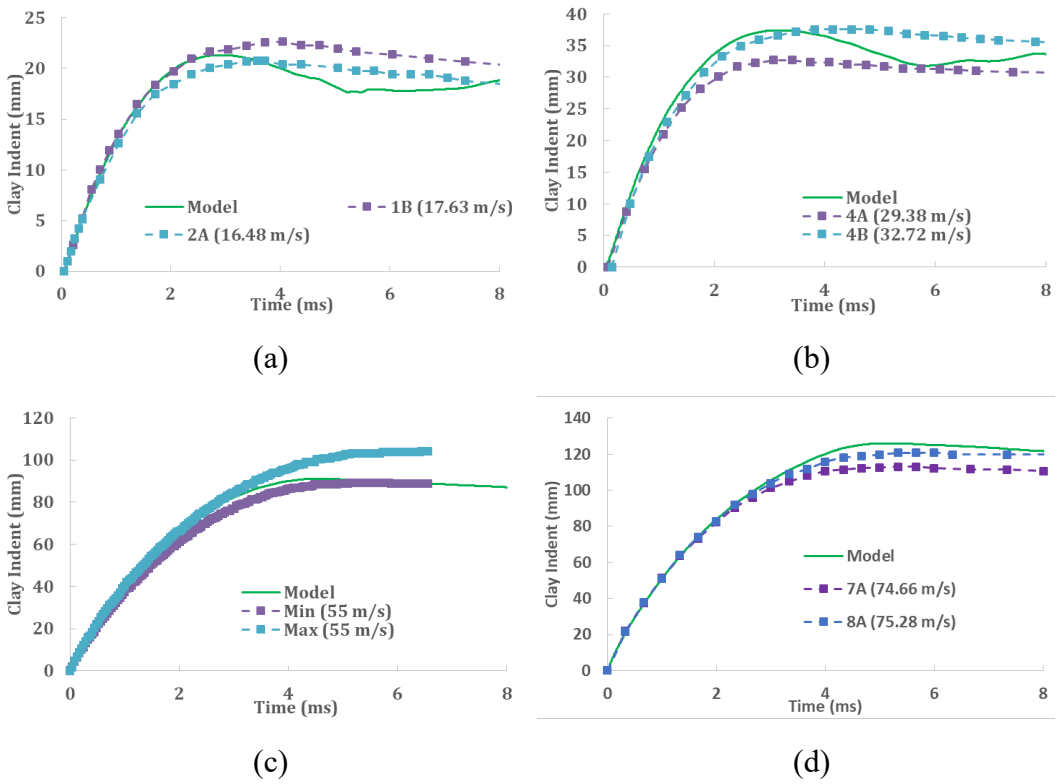

Fig. 27 Comparison between models and impact tests for (a) low velocity, (b) medium velocity, (c) 55 m/s, and (d) high velocity

4. Conclusions and Discussions

First the previous DEVCOM ARL clay model was reviewed. The compressive stress-strain curve for the material model was taken from the compression tests at a rate of 0.007/s, closest test data to quasi-static conditions. A set of parameters, including the tensile stress-strain curve and strain-rate scaling factors, were obtained from the parametric study to best match the test data. However, only the residual clay indents were measured in the drop tests, and the time history of clay indent in the impact tests of 55 m/s did not show rebound. The previous DEVCOM ARL clay model did not account for clay rebound.

In this study, additional drop and impact tests were conducted to evaluate the clay rebound and previous DEVCOM ARL clay model. High-speed cameras were used to capture the time history of clay indent in the drop tests. The impact tests were also conducted at three other impact velocities. The test data showed that the clay rebound existed for both drop and impact tests, and the percentage of rebounds can be as high as 15%. For the impact tests, the percentage of rebounds decreased with the impact velocity and the rebound was almost negligible for impact velocity of 55 m/s and higher, which agreed with previous tests.

Since the percentage of rebound cannot be ignored, the material model for the clay was recalibrated in this work. The same material model was used for the clay, but the parameters were adjusted to capture the rebound. Parametric study indicated the tensile Young's modulus was the main parameter to affect the clay rebound. A new set of material parameters were obtained to best match the test data. The model had good agreements of the peak indents and magnitude of rebound for both the drop and impact tests; however, the rate of rebound was not captured for the impact tests. Therefore, the model could not accurately predict the dynamic response after its peak value, but could reasonably predict the peak and residual indents. The recalibrated clay model is very critical to numerical modeling of clay response under impact loadings for the behind armor blunt trauma analysis.

5. References

ATC (US Army Aberdeen Test Center). TOP 10-2-210. Ballistic testing of hard body armor using clay backing. Aberdeen Test Center; 2008.

Buchely MF, Maranon A, Silberschmidt VV. Material model for modeling clay at high strain rates. International Journal of Impact Engineering. 2016;90:1–11.

Callahan JE. Analysis of composite helmet impact by the finite element method, Master's thesis. Virginia Polytechnic Institute and State University; 2011.

Carton E, Roebroeks G, Broos H, Halls V, Zheng J. Characterization of dynamic properties of ballistic clay. Personal Armour Systems Symposium, Robinson College; 2014 Sep 8–12.

Chijiiwa K, Hatamura Y, Hasegawa N. Characteristics of plasticine used in the simulation of slab in rolling and continuous-casting. Transactions of the Iron and Steel Institute of Japan. 1981;21(3):178–186.

Chua C-K, Chen Y-L. Ballistic-proof effects of various woven constructions. Fibres & Textiles in Eastern Europe. 2010;18(6 [83]):63–67.

Hernandez C, Buchely MF, Maranon A. Dynamic characterization of Roma Plastilina No. 1 from drop test and inverse analysis. International Journal of Mechanical Sciences. 2015;100:158–168.

Ivancik J, Mrozek R. Joint live fire (JLF) report for penetration profiles of ballistic backing materials for body armor testings. US Army Research Laboratory; 2017 Feb 10.

Laible RC. Ballistic materials and penetration mechanics. Elsevier Scientific Publishing Company; 1980.

Li YQ, Gao X-L, Fournier AJ, Sherman SA. Two new penetration models for ballistic clay incorporating strain-hardening, strain-rate and temperature effects. International Journal of Mechanical Sciences. 2019;151:582–594.

LS-DYNA keyword user's manual, vol II, material models. Livermore Software Technology Corporation (LSTC); 2016 July.

Mates SP, Forster A, Riley M, Rice K. Mechanical behavior of ballistic clay as a function of temperature, pressure and strain rate. Proceedings of the Personal Armour Systems Symposium 2014, 2014 Sep 8–12.

Prather R, Swann C, Hawkins C. Backface signatures of soft body armors and the associated trauma effects. Edgewood Arsenal (US); 1977. Report No. ARCSL-TR-77055.

Rafaels K, Good C, Loftis K, Satapathy S, Schuster B, Zhang TG, McDonald J, Jannotti P, DeBonis D, Baumer T, et al. Assessment of change in behind-armor blunt trauma (BABT) criteria. DEVCOM Army Research Laboratory (US); 2019 Mar. Report No.: ARL-TR-8670.

Sofuoglu H, Rasty J. Flow behavior of plasticine used in physical modeling of metal forming processes. Tribology International. 2000;33(8):523–529.

van der Jagt-Deutekom MJ, Carton EP, Philippens MMGM. Separation phenomena between armour plate and clay backing during projectile impact. TNO; 2012. TNO Report No. TNO 2012 R10755.

Zhang TG, Ivancik J, Mrozek RA, Satapathy SS. Material characterization of ballistic Roma Plastilina no. 1 clay. Proceedings of the 30th International Symposium on Ballistics; 2017 Sep 11–15.

List of Symbols, Abbreviations, and Acronyms

ARL	Army Research Laboratory
DEVCOM	US Army Combat Capabilities Development Command
DIC	Digital Image Correlation
DOP	depth of penetration
fps	frames per second
PPE	personal protective equipment
RP #1	Roma Plastilina No. 1

1 (PDF) DEFENSE TECHNICAL INFORMATION CTR DTIC OCA

1 (PDF) DEVCOM ARL
FCDD RLD DCI
TECH LIB

7 (PDF) DEVCOM SC
D COLANTO
R DILALLA
J FONTECCHIO
B FASEL
J KIREJCZYK
M MAFEO
J PARKER

3 (PDF) PEO SOLDIER
C BAKER
J HOPPING
J MULLENIX

43 (PDF) DEVCOM ARL
FCDD RLC ED
S O'BRIEN
FCDD RLH BA
A EIDSMORE
FCDD RLW
S KARNA
A RAWLETT
S SCHOENFELD
J ZABINSKI
FCDD RLW B
C HOPPEL
P GILLICH
FCDD RLW MA
T BOGETTI
S BOYD
T PLAISTED
J STANISZEWSKI
E WETZEL
M YEAGER
FCDD RLW T
R FRANCART
FCDD RLW TA
S BILYK
M GRAHAM
FCDD RLW TB
S ALEXANDER
R BANTON
T BAUMER
A BROWN
B FAGAN
A GOERTZ
A GUNNARSSON
C HAMPTON
R KARGUS
D KRAYTERMAN
M KLEINBERGER
E MATHEIS
J MCDONALD
P MCKEE
K RAFAELS
S SATAPATHY
M TEGTMEYER
C WEAVER
T WEERASOORIYA
S WOZNIAK
T ZHANG
FCDD RLW TC
J CAZAMIAS
FCDD RLW TD
B KRZEWINSKI
FCDD RLW TE
P SWOBODA
FCDD RLW PG
N GNIAZDOWSKI